

## Near-IR subwavelength microdisk lasers

Q. Song,<sup>1</sup> H. Cao,<sup>1,a)</sup> S. T. Ho,<sup>2</sup> and G. S. Solomon<sup>3</sup>

<sup>1</sup>Department of Applied Physics, Yale University, New Haven, Connecticut 06520-8482, USA

<sup>2</sup>Department of Electrical Engineering and Computing Science, Northwestern University, Evanston, Illinois 60208, USA

<sup>3</sup>Atomic Physics Division, NIST, Gaithersburg, Maryland 20899-8423, USA

(Received 13 October 2008; accepted 23 January 2009; published online 10 February 2009)

We report single-mode lasing in subwavelength GaAs disks under optical pumping. The disks are fabricated by standard photolithography and two steps of wet chemical etching. The simple fabrication method can produce submicron disks with good circularity, smooth boundary, and vertical sidewalls. The smallest lasing disks have a diameter of 627 nm and thickness of 265 nm. The ratio of the disk diameter to the vacuum lasing wavelength is about 0.7. Our numerical simulations confirm that the lasing modes are whispering-gallery modes with the azimuthal number as small as 4 and a modal volume of  $0.97(\lambda/n)^3$ . © 2009 American Institute of Physics.

[DOI: 10.1063/1.3081106]

Subwavelength laser sources have important applications to nanophotonic circuits, on-chip optical interconnects, and very local chemical and biological sensing. Semiconductor microlaser resonators based on photonic crystals or Bragg mirrors can attain subwavelength modal volumes but require the overall sizes of feedback structures at least several times larger than the wavelength.<sup>1,2</sup> Metallic coatings provide stronger confinement of light and consequently higher device-packing density.<sup>3-5</sup> Surface plasmon waveguides have been exploited for terahertz quantum cascade lasers with all three dimensions smaller than the vacuum emission wavelength.<sup>6,7</sup> The dissipative loss of metal at optical and near-IR frequencies, however, is much higher than that at terahertz. Lasing at near-IR is realized in three-dimensional (3D) subwavelength metal-coated cavities at low temperature where the metal absorption is reduced.<sup>3</sup> Even at 10 K, the cavity quality ( $Q$ ) factor is only a couple of hundreds, limited by the dissipative loss of metal. Another promising candidate for subwavelength laser resonators is the dielectric disk. It has small cavity size and high  $Q$  factor because light is confined by total internal reflection at the disk edge.<sup>1</sup> To avoid high optical bend losses in small disks, most microdisk lasers have a diameter over 1  $\mu\text{m}$ .<sup>8,9</sup> Recently Zhang *et al.*<sup>10</sup> have realized visible submicron disk lasers, which operate at room temperature. The smallest disks they obtain by lasing have the diameter of 645 nm, which is equal to the lasing wavelength in vacuum. In addition to the cavity size, the fabrication cost is also an important factor for practical applications. The submicron-scale lasers are fabricated by electron-beam lithography and dry etching. Although it gives good control of cavity shape and surface roughness, such fabrication method makes mass production nearly impossible.

In this letter, we report lasing in subwavelength GaAs disks at near-IR frequency. The disks are fabricated by standard photolithography and two steps of wet chemical etching. The submicron disks have good circularity, smooth boundary, and vertical sidewall. Single mode lasing is obtained by optical pumping. The gain is provided by the wet-

ting layers of InAs quantum dots (QDs) embedded in the GaAs disks. The diameter of the smallest lasing disks is 627 nm, which is about 30% smaller than the vacuum lasing wavelength. The 3D finite-difference time-domain (FDTD) calculations show that the lasing modes in the subwavelength disks are whispering-gallery modes (WGMs) with the azimuthal number  $m=4$  or 5. The GaAs disk laser with diameter 627 nm and thickness 265 nm is the smallest dielectric disk laser that has been reported so far. Our simple fabrication method provides the opportunity for high-throughput production of the ultrasmall lasers.

The sample is grown on a GaAs substrate by molecular beam epitaxy. The layer structure consists of 1000 nm  $\text{Al}_{0.68}\text{Ga}_{0.32}\text{As}$  and 265 nm GaAs. Inside the GaAs layer there are 6 ML of InAs QDs equally spaced by 25 nm GaAs barriers. Standard photolithography is used to define circular patterns of diameter 3–5  $\mu\text{m}$  within the photoresist (PR). Then GaAs and AlGaAs are etched nonselectively in a mixture of  $\text{HBr}:\text{H}_2\text{O}_2:\text{H}_2\text{O}$  with the ratio 4:1:25. The etching is isotropic, leading to an undercut of GaAs beneath the PR mask. In the case of a large etch depth, the diameter of GaAs disk is significantly smaller than that of the PR disk. By increasing the etch time, we reduce the GaAs disk diameter to submicron. To obtain a fine control of the etch depth, we slow down the etching process by placing the etch solution in an ice bath. For a typical etch depth of 2.4  $\mu\text{m}$ , the etch time is increased from 1 min at room temperature to 28 min at 5 °C. Finally, dilute HF is used to selectively etch  $\text{Al}_{0.68}\text{Ga}_{0.32}\text{As}$ , forming a pedestal underneath the GaAs disk.

Figure 1(a) is a top-view scanning electron microscope (SEM) image of a GaAs disk. The disk diameter  $d=627$  nm is much smaller than that of the PR mask ( $\sim 5$   $\mu\text{m}$ ). Despite of a large undercut of GaAs, the circular disk shape is well kept. The tilt-view SEM image in Fig. 1(b) shows that the sidewall of GaAs disk is vertical and smooth. As compared to dry etching, wet chemical etching creates less surface damage. The top diameter of  $\text{Al}_{0.68}\text{Ga}_{0.32}\text{As}$  pedestal is about 260 nm. The dimension of the pedestal is set to minimize light leakage to the GaAs substrate, while maintaining acceptable heat sink for the GaAs disk. The surface of pedestal in Fig. 1(b) is rough possibly due to As passivation in the selective etching process.

<sup>a)</sup>Electronic mail: hui.cao@yale.edu.

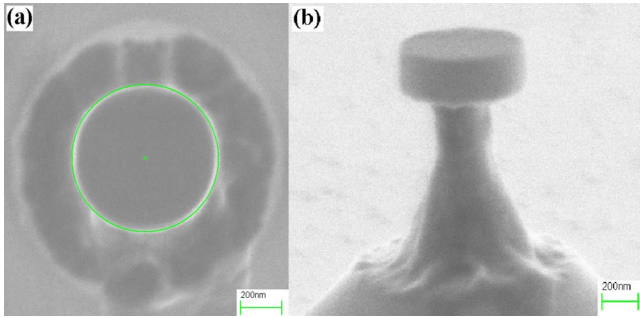


FIG. 1. (Color online) (a) Top-view and (b) tilt-view scanning electron microscope images of a GaAs disk on top of an AlGaAs pedestal. The disk diameter is 627 nm and the disk thickness is 265 nm. The green circle is a fit of the disk shape.

In the lasing experiment, the microdisks are optically pumped by a mode-locked Ti:Sapphire laser (pulse width = 200 fs, center wavelength = 800 nm, pulse repetition rate = 76 MHz). The sample is cooled to 10 K in a liquid helium cryostat. A long-working-distance objective lens focuses the pump beam to a single disk. Emission from the disk is collected by the same objective lens and directed to a half-meter spectrometer with a liquid nitrogen cooled charge-coupled device array detector. Figure 2 shows the measurement results of a GaAs disk with  $d=722$  nm and thickness 265 nm. At low pumping level, radiative recombination of carriers in the InAs QDs and the wetting layers produce spontaneous emission in the wavelength ranges of 890–950 and 860–880 nm, respectively. Figure 2(a) shows the spectra of emission from the wetting layers when the incident pump power  $P$  is varied from 39 to 91  $\mu\text{W}$ . For  $P \geq 50$   $\mu\text{W}$ , a narrow peak appears at wavelength  $\lambda=865$  nm. Figure 2(b) is a logarithmic plot of the spectrally integrated intensity  $I$  of the peak versus  $P$ . The curve exhibits a  $S$ -shape with two kinks at  $P \approx 70$   $\mu\text{W}$  and 160  $\mu\text{W}$ . Below the first kink, the slope of  $\log I$  over  $\log P$  is approximately 0.91, indicating a linear increase in peak intensity with pumping. Above the first kink, the slope changes to 3.6. The superlinear increase in  $I$  with  $P$  results from optical amplification. Above the second kink the slope changes back to 0.92 due to gain saturation.

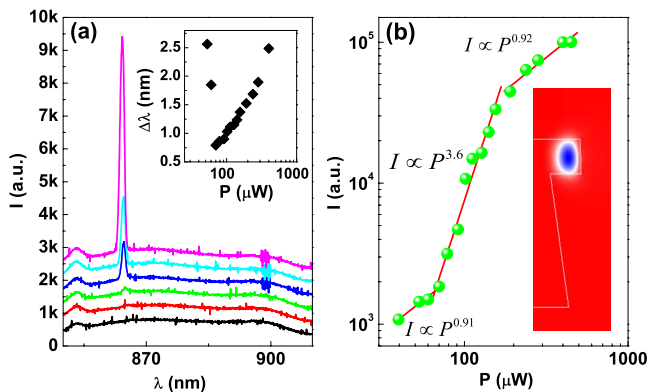


FIG. 2. (Color online) (a) Spectra of InAs wetting layer emission from a GaAs disk of diameter 722 nm. From bottom to top, the incident pump power  $P=39, 53, 60, 70, 78.5, 91.5$   $\mu\text{W}$ . The spectra were vertically shifted for a clear view. Inset: linewidth of lasing peak vs pump power. (b) Log-log plot of the spectrally integrated intensity  $I$  of the narrow peak at  $\lambda=860$  nm as a function of pump power  $P$ . The straight lines are fitted curves. Inset: calculated spatial distribution of magnetic field component normal to the disk plane for a TE-polarized WGM in this microdisk.

Such behavior confirms lasing action in this disk, which has all three dimensions smaller than the lasing wavelength in vacuum. The inset of Fig. 2(a) is a plot of the linewidth  $\Delta\lambda$  of lasing peak versus  $P$ .  $\Delta\lambda$  decreases quickly to 0.7 nm as  $P$  increases to 70  $\mu\text{W}$ , and then starts increasing. This increase is attributed mostly to temporal shift in lasing frequency.<sup>11</sup> The short pump pulses generate hot carriers in the GaAs barriers which subsequently relax to the InAs wetting layers and QDs. The carrier distribution keeps changing in time during the short lasing period following the pump pulse. Consequently the refractive index changes in time, causing a continuous redshift in lasing frequency.<sup>12</sup> In our time-integrated measurement of lasing spectrum, the transient frequency shift results in a broadening of lasing line. Such broadening increases with the hot carrier density and becomes dominant at higher pumping. It leads to an increase in  $\Delta\lambda$  with  $P$  above 70  $\mu\text{W}$ .

To identify the lasing mode, we calculate numerically the resonant modes in the subwavelength disk by solving the Maxwell's equations in 3D with the FDTD method and utilizing the rotational symmetry. In calculation, we focus on the modes predominately TE polarized, which are similar to the lasing modes observed experimentally. For the disk of diameter 722 nm and thickness 265 nm, a WGM with the azimuthal number  $m=5$  and radial number  $l=1$  is found at  $\lambda \approx 860$  nm. It is very close to the wavelength of the observed lasing mode. The calculated  $Q$  factor of this mode is about 4000. The surface roughness and slight shape deformation of the disk are not taken into account in the calculation, which would degrade the  $Q$  factor. The calculated spatial distribution of magnetic field in the cross-section of disk and pedestal is shown as inset in Fig. 2(b). It is evident that the mode is concentrated near the GaAs disk edge and has little overlap with the  $\text{Al}_{0.68}\text{Ga}_{0.32}\text{As}$  pedestal. Our simulations confirm that a fine control of the pedestal size is crucial to minimize light leakage through the pedestal to the substrate as well as the scattering loss caused by the pedestal surface roughness. The modal volume is calculated to be approximately  $1.3(\lambda/n)^3$ . Because of the small cavity size, the frequency spacing of high- $Q$  modes well exceeds the gain bandwidth. To achieve lasing, it is important to fine tune the disk diameter so that one of the high- $Q$  mode overlaps with the gain spectrum.

We also calculate the  $Q$  values for WGMs with  $l=1$  but different  $m$  in the subwavelength disk. The  $Q$  factor drops quickly from over 10 000 to 100 when  $m$  decreases from 6 to 3 because of the dramatic increasing of light leakage through tunneling at the disk boundary. For  $m=4$ ,  $Q \approx 700$ . To check experimentally whether we can achieve lasing in the WGM with  $m=4$ , we fabricate a GaAs disk of diameter 627 nm and thickness 265 nm (shown in Fig. 1). The WGM with  $m=4$  in this disk coincides with the gain spectrum of InAs wetting layer. We observe the onset of lasing action at the incident pump power  $P=220$   $\mu\text{W}$ . The inset of Fig. 3(b) shows the lasing peak at  $\lambda=870$  nm. A threshold behavior is clearly seen in the growth of peak intensity with pumping [Fig. 3(a)]. Figure 3(b) is a plot of the peak width  $\Delta\lambda$  versus  $P$ .  $\Delta\lambda$  first decreases with increasing  $P$ , then saturates at higher  $P$ . The minimal linewidth is about 1.7 nm. Our numerical simulation reveals its modal volume is  $0.97(\lambda/n)^3$ . The higher lasing threshold and broader linewidth are attributed to the

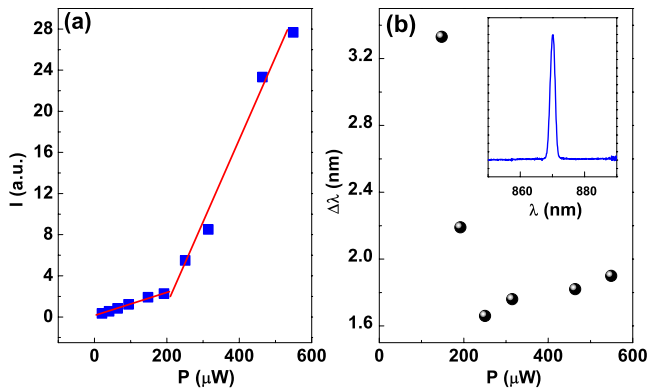


FIG. 3. (Color online) (a) Linear plot of the lasing peak intensity vs the incident pump power  $P$  for the GaAs disk shown in Fig. 1. The straight lines are fitted curves. (b) Spectral width  $\Delta\lambda$  of the lasing peak as a function of pump power  $P$ . Inset: the emission spectrum at  $P=300 \mu\text{W}$  showing the lasing peak.

smaller size and lower quality of this disk as compared to the previous disk with  $d=722 \text{ nm}$ .

In conclusion, we demonstrate single-mode lasing in submicron-scale GaAs disks in the wavelength range of 860–880 nm. The disks, fabricated by standard photolithography and two steps of wet chemical etching, have good circularity and smooth and vertical sidewalls. Both the disk diameter  $d$  and thickness are smaller than the lasing wavelength  $\lambda$  in vacuum. The smallest lasing disks have the ratio  $d/\lambda \approx 0.7$ . The lasing modes are WGMs with the azimuthal number

$m=4$ . The modal volume is  $0.97(\lambda/n)^3$ . Such ultrasmall lasers have potential applications in high-density photonic circuits and microscale chemical or biological sensing systems. The simple fabrication method facilitates mass production of the subwavelength disk lasers.

This work is supported partly by NIST under the Grant No. 70NANB6H6162 and by NSF under the Grant No. ECCS-0823345.

<sup>1</sup>K. J. Vahala, *Nature (London)* **424**, 839 (2003).

<sup>2</sup>Y. Akahane, T. Asano, B.-S. Song, and S. Noda, *Nature (London)* **425**, 944 (2003).

<sup>3</sup>M. T. Hill, Y. S. Oei, B. Smalbrugge, Y. Zhu, T. De Vries, P. J. Van Veldhoven, F. W. M. Van Otten, T. J. Eijkemans, J. P. Turkiewicz, H. De Waardt, E. J. Geluk, S. H. Kwon, Y. H. Lee, R. Notzel, and M. K. Smit, *Nat. Photonics* **1**, 589 (2007).

<sup>4</sup>C. Manolatou and F. Rana, *IEEE J. Quantum Electron.* **44**, 435 (2008).

<sup>5</sup>A. Mizrahi, V. Lomakin, B. A. Slutsky, M. P. Nezhad, L. Feng, and Y. Fainman, *Opt. Lett.* **33**, 1261 (2008).

<sup>6</sup>Y. Chassagneux, J. Palomo, R. Colombelli, S. Dhillon, C. Sirtori, H. Beere, J. Alton, and D. Ritchie, *Appl. Phys. Lett.* **90**, 091113 (2007).

<sup>7</sup>L. A. Dunbar, R. Houdre, G. Scalari, L. Sirigu, M. Giovannini, and J. Faist, *Appl. Phys. Lett.* **90**, 141114 (2007).

<sup>8</sup>A. F. J. Levi, S. L. McCall, S. J. Pearton, and R. A. Logan, *Electron. Lett.* **29**, 1666 (1993).

<sup>9</sup>T. Baba *IEEE J. Sel. Top. Quantum Electron.* **3**, 808 (1997).

<sup>10</sup>Z. Y. Zhang, L. Yang, V. Liu, T. Hong, K. Vahala, and A. Scherer, *Appl. Phys. Lett.* **90**, 111119 (2007).

<sup>11</sup>G. Pompe, T. Rappen, M. Wehner, F. Knop, and M. Wegener, *Phys. Status Solidi B* **188**, 175 (1995).

<sup>12</sup>F. Jahnke and S. W. Koch, *Phys. Rev. A* **52**, 1712 (1995).